Physics and Chemistry of Minerals (2019) 46:333–341
https://doi.org/10.1007/s00269-018-1006-6

ORIGINAL PAPER

Compressional behavior of natural eclogitic zoisite by synchrotron X-ray single-crystal diffraction to 34 GPa

Jingui Xu[1] · Dongzhou Zhang[2] · Dawei Fan[1] · Xiang Wu[3] · Feng Shi[3] · Wenge Zhou[1]

Received: 3 July 2018 / Accepted: 24 September 2018 / Published online: 8 October 2018

Abstract

Zoisite is a typical accessory mineral of eclogite; understanding its compressional behavior is important for the knowledge of the properties and processes within subduction zones. In this study, the compressional behavior of a natural eclogitic zoisite $Ca_{1.99}(Al_{2.87}Fe_{0.11})Si_{3.00}O_{12}OH$ was investigated at ambient temperature and high pressure to 34 GPa, using a diamond anvil cell (DAC) combined with synchrotron-based single-crystal X-ray diffraction (XRD) method. Our results indicate that zoisite is stable over the experimental pressure range. The pressure–volume (*P*–*V*) data were fitted to a third-order Birch–Murnaghan equation of state (BM3 EoS), and the equation of state coefficients including zero-pressure unit-cell volume (V_0), isothermal bulk modulus (K_{T0}), and its pressure derivative (K'_{T0}) were obtained as: $V_0 = 904.77(8)$ Å^3, $K_{T0} = 118(1)$ GPa, and $K'_{T0} = 6.3(2)$, respectively. The axial compressibilities (β) for *a*-, *b*-, and *c*-axes were also obtained using a parameterized form of the BM3 EoS, and the results show $\beta_{a0} < \beta_{b0} < \beta_{c0}$ with $\beta_{a0}:\beta_{b0}:\beta_{c0} = 1:1.28:1.50$. In addition, the bulk modulus of this study is very consistent with previously studied zoisite with similar Fe content. However, the axial compressibility is significantly different with the previous study and the compression of zoisite in this study is more isotropic, which may result from the difference in the pressure-transmitting medium.

Keywords Zoisite · High pressure · Synchrotron single-crystal X-ray diffraction · Diamond anvil cell · Hydrous minerals

Introduction

Zoisite is a hydrous mineral that belongs to the disilicates and epidote-group minerals. Unlike other epidote-group minerals, zoisite is orthorhombic (*Pnma* space group) instead of monoclinic (Nesse 2000). The crystal structure of zoisite has been described in great details (e.g., Dollase 1968; Nesse 2000), since it was first determined by Fesenko et al. (1955). Its general chemical formula can be described by A1A2M12M3O$(TO_4)(T_2O_7)$(OH), where the A site is seven coordinated, the M site is octahedrally coordinated, and T site is tetrahedrally coordinated (Fig. 1). The A, M, and T sites are commonly occupied by Ca^{2+}, Al^{3+}, and Si^{4+}, respectively (Franz and Liebscher 2004), while natural specimens can contain small amounts of other cations like Sr^{2+}, Mn^{2+}, Fe^{3+}, Cr^{3+}, etc (Alvaro et al. 2012; Franz and Liebscher 2004; Nagasaki and Enami 1998). Ghose and Tsang (1971) investigated the ordering of small amounts of Mn^{2+} and Fe^{3+} ions in zoisite, and suggested that Mn^{2+} and Fe^{3+} are ordered and located in the A1 and M3 sites, respectively, and commonly Fe^{3+} in natural zoisite occupy no more than 10% of the M sites (Nesse 2000). The substitution of Fe^{3+}–Al^{3+} of the synthetic zoisite [composition range: $X_{Fe} = 0.00$–0.14, where $X_{Fe} = Fe^{3+}/(Fe^{3+} + Al^{3+} - 2)$] was investigated by Liebscher et al. (2002), and an isosymmetric displacive phase transition was found at $X_{Fe} = 0.05$. In addition, Dörsam et al. (2007) studied the substitution of Sr^{2+}–Ca^{2+} in A sites within $X_{Sr} = 0.06$-1 [$X_{Sr} = Sr/(Ca+Sr)$] and found that the lattice parameters of zoisite increase linearly with increasing Sr content.

Electronic supplementary material The online version of this article (https://doi.org/10.1007/s00269-018-1006-6) contains supplementary material, which is available to authorized users.

✉ Wenge Zhou
zhouwenge@vip.gyig.ac.cn

[1] Key Laboratory for High-Temperature and High-Pressure Study of the Earth's Interior, Institute of Geochemistry, Chinese Academy of Sciences, Guiyang 550081, China

[2] Hawaii Institute of Geophysics and Planetology, University of Hawaii at Manoa, Honolulu, HI 96822, USA

[3] State Key Laboratory of Geological Processes and Mineral Resources, China University of Geoscience, Wuhan 430074, China

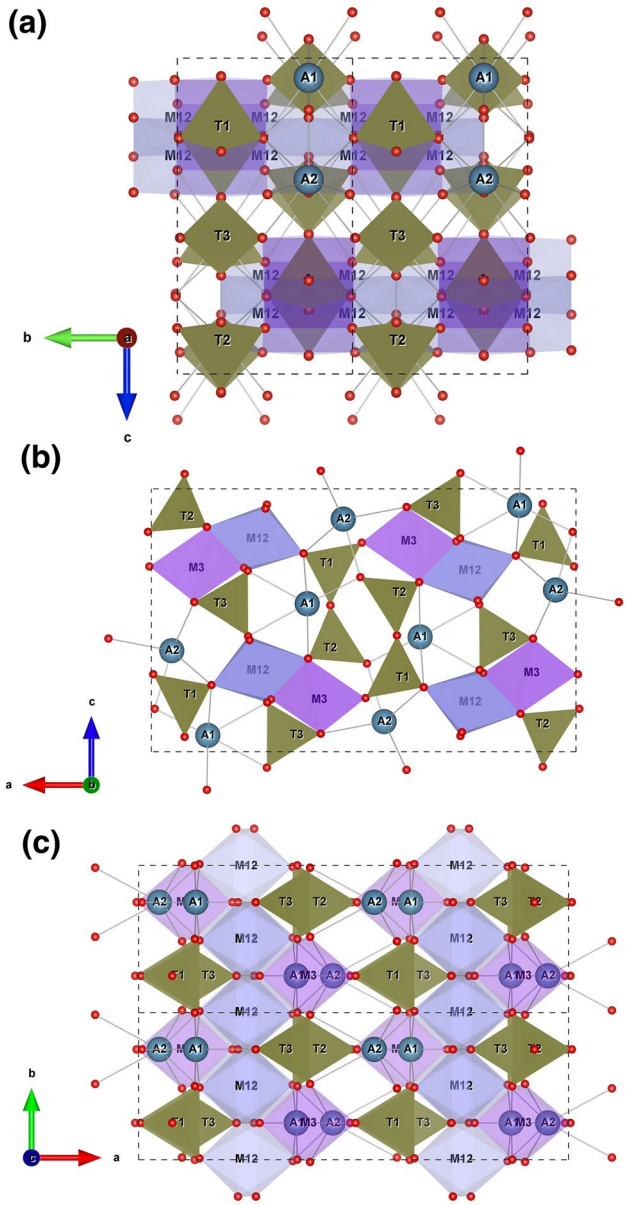

Fig. 1 Crystal structure of zoisite, viewed along the *a*-axis (**a**), *b*-axis (**b**), and *c*-axis (**c**); the red balls indicate the oxygens. In this structure, T1, T2, and T3 represent tetrahedral sites that commonly occupied by Si^{4+}. M12 and M3 represent two types of octahedral sites; M12 is occupied by Al^{3+}, while M3 can be occupied by Al^{3+} and Fe^{3+}. A1 and A2 indicate two distinct seven-coordinated sites occupied by Ca^{2+} (color online)

Zoisite is also a geologically important mineral, it commonly occurs in metamorphic rocks like schist, amphibolite, and eclogite (Enami et al. 2004). It has been thought to be an important carrier of water and trace elements such as Sr in subducted oceanic crust (Nicholls and Ringwood 1973; Spandler et al. 2003). Therefore, several studies have been conducted on the pressure–temperature (*P–T*) stability field of zoisite, and the maximum pressure stability was reached to 6.6 GPa at 950 °C (e.g., Boettcher 1970; Poli and Schmidt 1998; Schmidt and Poli 2004). In addition, the elastic behaviors of zoisite were also studied. Comodi and Zanazzi (1997) investigated the compressional behavior of zoisite with composition Ca_2Al_2 $(Al_{0.9}Fe_{0.1})Si_3O_{12}OH$ by the single-crystal XRD experiments in a DAC at ambient temperature. By fitting the pressure–volume (*P–V*) data to a third-order Birch-Murnaghan equation of state (BM3 EoS), they obtained bulk modulus and its pressure derivative was: $K_{T0} = 102(7)$ GPa, and $K'_{T0} = 4.8(4)$. Recently, Alvaro et al. (2012) measured the equation of state on two zoisite samples (Fe-free: $((Ca_{1.99}Sr_{0.01})(Al_{2.99}V_{0.01})Si_3O_{12}OH)$ and Fe-bearing: $((Ca_{1.99}Sr_{0.01})(Al_{2.88}Fe_{0.12})Si_3O_{12}OH)$) using DACs combined with the single-crystal XRD method, and obtained: $K_{T0} = 122.1(7)$ GPa, with $K'_{T0} = 6.8(2)$ for the Fe-free sample and $K_{T0} = 119.1(7)$ GPa with $K'_{T0} = 7.3(2)$ for the Fe-bearing sample. The elasticity of a Fe-free zoisite were also studied by Brillouin scattering at ambient conditions (Mao et al. 2007). Furthermore, high-pressure and high-temperature EoS studies were also conducted on natural [contains 2.3–4.3% of the ferric end-member, $Ca_2Al_2Fe^{3+}Si_3O_{12}(OH)$ (Pawley et al. 1998)] and synthetic [$Ca_2Al_3Si_3O_{12}(OH)$, (Grevel et al. 2000)] zoisites.

In this study, we conducted in situ synchrotron single-crystal XRD experiments on a natural eclogitic zoisite to explore its phase stability and equation of state extending to a much higher pressure (~34 GPa) than the previous studies under ambient temperature. This study will help us to understand the stability of zoisite under extremely cold conditions, such as those within the old and fast subducting slabs in subduction zones (like the Tonga slab) (Ganguly et al. 2009). In addition, the obtained elastic parameters are compared to the previous studies, and the potential implications of zoisite in the subduction zone are also discussed.

Materials and methods

A natural zoisite was collected from eclogite rocks of the Dabie–Sulu ultrahigh-pressure metamorphic belt, the Bixiling area in Yuexi County, Anhui Province, China. The chemical composition of the sample was determined by a JXA8230 electron microprobe with a 15 kV accelerating voltage and 20 nA beam current, and the beam size was 5 μm in diameter. The empirical formula is $Ca_{1.99}(Al_{2.87}Fe_{0.11})Si_{3.00}O_{12}OH$ (Table 1). A single crystal with size ca. 30 μm × 25 μm (less than 10 μm in thickness) was mounted onto a polymer holder for the ambient XRD experiments. After that, this crystal was loaded into a BX90 DAC equipped with a pair of diamonds with 300 μm culet size. A rhenium gasket pre-indented to a thickness of ~45 μm with a hole of 180 μm in diameter was used as the sample chamber. The Au powder was loaded as the pressure standard (Fei

Table 1 Chemical composition of zoisite based on the average of seven-point analyses

SiO_2	38.84(6)	Si	3.001
TiO_2	0.07(1)	Ti	0.004
Al_2O_3	31.54(23)	Al	2.871
Fe_2O_3	1.84(12)	Fe	0.107
MnO	0.01(1)	Mn	0.001
MgO	0.06(3)	Mg	0.007
CaO	24.14(17)	Ca	1.997
Na_2O	0.05(1)	Na	0.007
K_2O	0.00(0)	K	0.000
Cr_2O_3	0.06(1)	Cr	0.003
P_2O_5	0.00(0)	P	0.000
SrO	0.00(0)	Sr	0.000
Nd_2O_3	0.00(0)	Nd	0.000
Total	96.62		7.998

Data in the parentheses represent standard deviations

et al. 2007). The diffraction patterns of Au were collected before and after sample data collection for each pressure, and the average pressure values were used for EoS calculations. A small ruby sphere with ~ 10 μm in diameter was also loaded as the pressure indicator for gas loading with Ne as the pressure-transmitting medium using the GSECARS gas-loading system (Rivers et al. 2008). After the gas loading, the diameter of sample chamber was ~ 90 μm. The pressure of the sample chamber was increased using an automated pressure-driven membrane system.

The synchrotron single-crystal XRD experiments at ambient and high pressures were carried out with a six-circle diffractometer at 13-BM-C experimental station of the Advanced Photon Source, Argonne National Laboratory. The wavelength of the incident X-ray was 0.4340 Å, and the beam size was 15 μm × 20 μm. Diffraction images were acquired on a MAR165 CCD detector and calibrated using the ambient LaB_6 as the diffraction standard (Zhang et al. 2017). Wide and stepped φ-rotation exposures were collected for the single-crystal sample at each pressure, with an exposure time of 4 s/deg. The φ-rotation (the opening angle of the DAC is ± 28°) axis was horizontal and perpendicular to the incident X-ray direction. The diffraction images collected at each pressure were analyzed using the GSE_ADA software package, and the unit-cell parameters (Table 2) were refined using the RSV software (Dera et al. 2013).

The intensity data of zoisite at ambient conditions were collected for structural refinements. The crystal structure was refined using the SHELX software (Sheldrick 2008) via the Olex2 user interface (Dolomanov et al. 2009), starting from atomic coordinates of Dollase (1968). According to the chemical composition and previously reported zoisite structure model (Alvaro et al. 2012; Comodi and Zanazzi 1997; Dollase 1968; Dörsam et al. 2007; Liebscher et al. 2002), the A1, A2, M12, T1, T2, and T3 sites were set to be fully occupied by Ca^{2+}, Ca^{2+}, Al^{3+}, Si^{4+}, Si^{4+}, and Si^{4+}, respectively, while M3 sites were occupied by a mixture of Al^{3+} and Fe^{3+} with refinable ratio. The hydrogen (H) was not considered in the refinement like that, in the study of Alvaro et al. (2012), due to its invisibility under the X-ray diffraction. Cations occupying the same polyhedral site were set to share the same atomic displacement parameter values and fractional coordinates, and the refinements were performed with anisotropic displace parameters only for cations. Details of the structure refinement, polyhedral geometry parameters [calculated using VESTA program, Momma and Izumi (2011)], atomic coordinates, and displacement parameters are listed in the supplementary material Tables S1, S2, and S3.

Table 2 Unit-cell parameters of zoisite at different pressures

Pressure (GPa)	*a* (Å)	*b* (Å)	*c* (Å)	*V* (Å^3)
0.0001	16.2057(7)	5.5595(3)	10.0424(5)	904.77(8)
0.8(1)	16.165(4)	5.548(1)	10.023(2)	899.0(3)
2.2(3)	16.139(6)	5.524(1)	9.967(2)	888.6(4)
3.8(1)	16.081(7)	5.504(1)	9.926(2)	878.5(4)
4.8(1)	16.052(6)	5.490(1)	9.899(2)	872.4(3)
7.8(1)	15.972(13)	5.452(1)	9.829(4)	855.9(8)
11.6(1)	15.904(18)	5.410(2)	9.739(5)	837.8(11)
13.0(1)	15.860(13)	5.400(1)	9.717(4)	832.2(8)
17.4(1)	15.776(18)	5.363(2)	9.624(5)	814.2(11)
21.0(1)	15.705(16)	5.334(2)	9.569(5)	801.6(9)
24.0(1)	15.656(12)	5.305(2)	9.514(4)	790.1(8)
28.1(2)	15.589(16)	5.279(2)	9.468(5)	779.2(9)
30.5(1)	15.563(13)	5.264(1)	9.425(4)	772.1(8)
34.0(1)	15.516(10)	5.236(1)	9.400(4)	763.7(6)

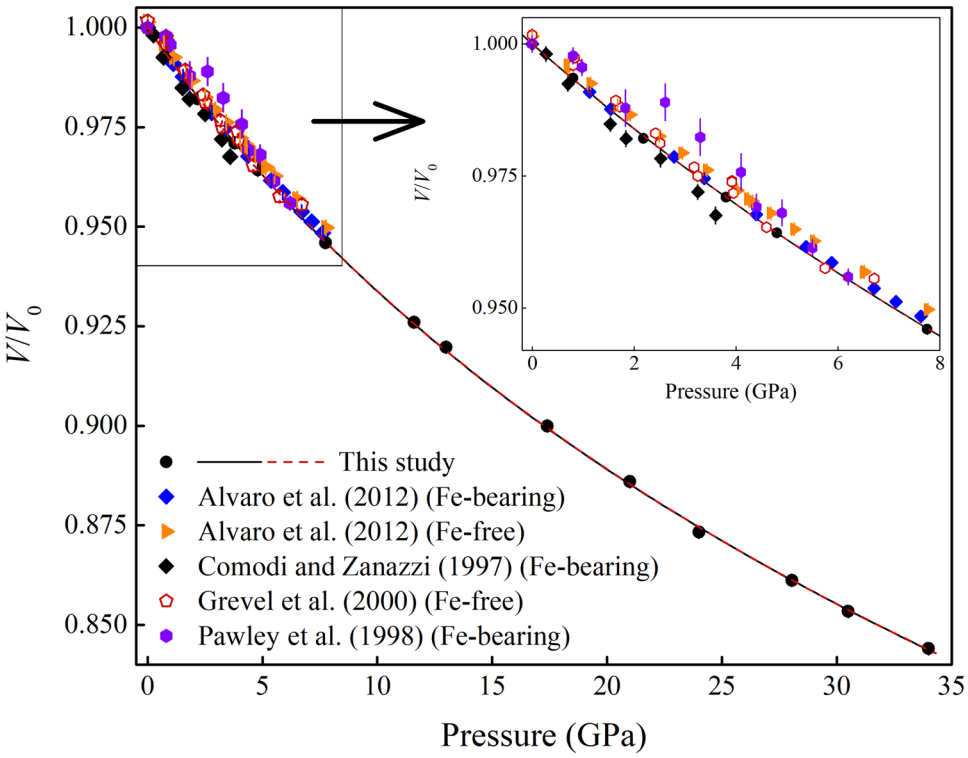

Fig. 2 Normalized unit-cell volume of zoisite as a function of pressure. The black solid line represents the BM3 EoS fitting based on all data of this study, and the red dotted line is the BM3 EoS-fitting curve based on high-pressure data only. The error bars are smaller than the symbols in this study. The insert figure shows the larger view of the data of the low-pressure range (color online)

Results and discussion

Equation of state of zoisite

No phase transitions were observed for zoisite over the experimental pressure range, as no abrupt changes in the lattice parameters as a function of pressure have been detected (Figs. 2, 3). The *P*–*V* data (Table 2) were fitted to the BM3 EoS, using the EoSFit7c program (Angel et al. 2014; Gonzalez-Platas et al. 2016). The coefficients were obtained as: $V_0 = 904.77(8)$ Å^3, $K_{T0} = 118(1)$ GPa, and $K'_{T0} = 6.3(2)$, with $\chi^2_w = 0.6$. Because of the ambient XRD data which were not collected in the BX90 DAC, we also performed the BM3 EoS fitting with the high-pressure *P*–*V* data only to check the consistency of the data collected at ambient and high-pressure conditions. The EoS coefficients were obtained as $V_0 = 904.74(35)$ Å^3, $K_{T0} = 118(2)$ GPa, and $K'_{T0} = 6.3(3)$, with $\chi^2_w = 0.6$. These values are nearly identical to the results derived from the fitting of all data. As shown in Fig. 2, the EoS curve derived from the fitting of the high-pressure data only is also very close to that obtained by fitting of all data. Therefore, the single-crystal XRD data collected at ambient and high-pressure conditions are consistent, and the EoS fitted with all data is more precise, as it gives the coefficients with smaller uncertainty. The normalized stress (F_E)–Eulerian strain (f_E) plot is shown in Fig. 4 (Angel (2000); $F_E = P/3f_E(1+2f_E)^{5/2}$, $f_E = [(V_0/V)^{2/3} - 1]/2$). F_E as a function of f_E has a positive slope, which is consistent with a value of K'_{T0} larger than 4 (Angel 2000). Therefore, the BM3 EoS is a reasonable choice of the EoS fitting of the *P*–*V* data (Angel 2000).

The EoS of zoisite in this study was compared to the literature results from high-pressure XRD studies (Fig. 2; Table 3). Several previous high-pressure XRD experimental studies have obtained the EoS coefficients of zoisite. As shown in Table 3, the $K_{T0} = 102(7)$ GPa obtained by Comodi and Zanazzi (1997) is much smaller than that of this study, although both zoisite samples have similar Fe content. In view of the higher uncertainty of K_{T0}, their determination of the bulk modulus likely suffered from the problems relating to the limited data amount and pressure range (0–4 GPa), and the difference in the pressure-transmitting medium may be another reason [Comodi and Zanazzi (1997) used a 16:3:1 methanol:ethanol:water mixture]. Pawley et al. (1998) measured the EoS of a natural zoisite and Grevel et al. (2000) measured the EoS of a synthetic zoisite, and both studies gave much higher K_{T0} values [127(4) and 125(2) GPa] than this study. Considering the data scatter, these two studies fixed the K'_{T0} to be 4 when determining the K_{T0}; however, refining three parameters including V_0, K_{T0}, and K'_{T0} which are required for a precise EoS determination (Angel 2000). Recently, Alvaro et al. (2012) reported a high-pressure single-crystal XRD study on two natural zoisite samples using DACs. The K_{T0} values were obtained as 122.1(7) and 119.1(7) GPa for the Fe-free and Fe-bearing zoisite, respectively. Their Fe-bearing

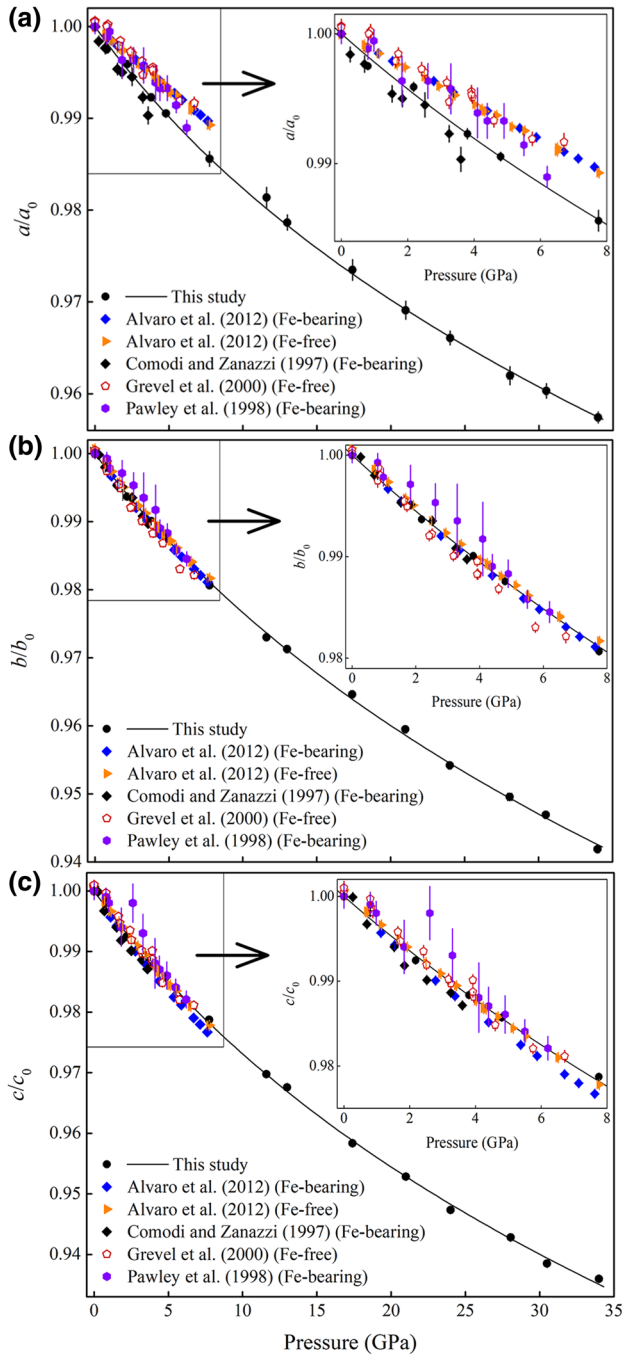

Fig. 3 Pressure dependence of the lattice parameters *a* (**a**), *b* (**b**), and *c* (**c**) of zoisite. The solid lines represent the BM3 EoS-fitting curves based on all data of this study. The insert figure in each graph shows the larger view of the data of the low-pressure range (color online)

zoisite has similar Fe content to this study, and the bulk modulus is consistent with this study [118(1) GPa] within the uncertainty (see also Fig. 2; Table 3).

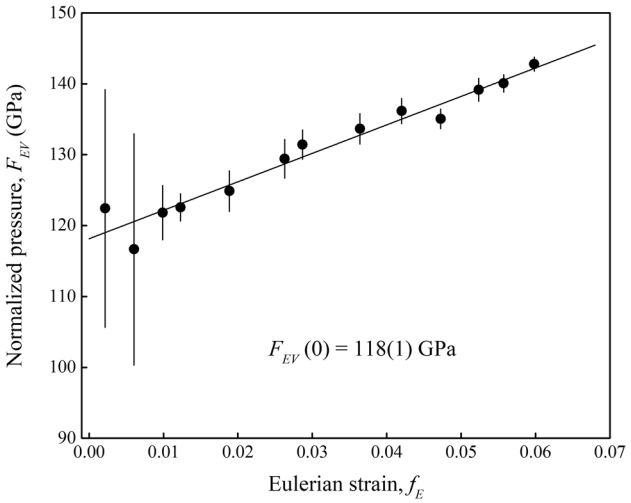

Fig. 4 Eulerian strain-normalized pressure (F_E–f_E) plot of the unit-cell volume of zoisite. The straight line represents the weighted linear fit of the F_E–f_E data, and the intercept value is F_{EV} (0) = 118(1) GPa

Axial compression of zoisite

The compressional data of the unit-cell parameters *a, b*, and *c* of zoisite were also fitted to a linear form of the BM3 EoS, to obtain the axial compressibilities, again using the EoSFit7c program (Angel et al. 2014; Gonzalez-Platas et al. 2016). The F_E–f_E plots also indicate that the *P-a, b, c* data can be reasonably described by the BM3 EoS (Fig. 5). The obtained linear BM3 EoS-fitting parameters of zoisite are listed in Table 4. In addition, the compressibilities [$\beta_{l0} = -(l^{-1})(\delta d/\delta P)_{P=0}$, Angel (2000)] of each axis at zero pressure were calculated as β_{a0}:β_{b0}:β_{c0} = 1:1.28:1.50, which shows that *c* has the highest compressibility and *b* is more compressible than *a* (Table 4).

We also compared the axial compressibility of zoisite in this study to the previous studies (Table 5). To made significative comparisons, here, we compared our results only to the compressional studies from Comodi and Zanazzi (1997) and Alvaro et al. (2012), as these studies were conducted using DACs combined with the single-crystal XRD method, and the zoisite samples have similar Fe contents (X_{Fe} = 0.10–0.12). In addition, the used pressure-transmitting media including the methanol–ethanol mixture, methanol–ethanol–water mixture, and Ne can retain good hydrostatic compressions within the pressure ranges (Angel et al. 2007; Klotz et al. 2009). As shown in Table 5, the axial compression anisotropy of zoisite in this study is very close to that of Comodi and Zanazzi (1997), although the axial compressions are different each other (Fig. 3). The compressions of *a*- and *c*-axes in this study are notably lower than that of the study by Comodi and Zanazzi

Table 3 BM3 EoS-fitting coefficients of zoisite

Sample descriptions	V_0 (Å^3)	K_{T0} (GPa)	K'_{T0}	Reference
[a]Natural	903.6(4)	102(7)	4.8(4)	Comodi and Zanazzi (1997)
[b]Natural	907(1)	127(4)	4[fixed]	Pawley et al. (1998)
[c]Synthetic	901.0(9)	125(2)	4[fixed]	Grevel et al. (2000)
[d]Natural	903.39(5)	122.1(7)	6.8(2)	Alvaro et al. (2012)
[e]Natural	906.95(5)	119.1(7)	7.3(2)	Alvaro et al. (2012)
[f]Natural	904.77(8)	118(1)	6.3(2)	This study

[a]$Ca_2Al_2(Al_{0.9}Fe_{0.1})Si_3O_{12}OH$
[b]$Ca_2Al_2(Al_{0.96}Fe_{0.04})Si_3O_{12}OH$
[c]$Ca_2Al_3Si_3O_{12}OH$
[d]$(Ca_{1.99}Sr_{0.01})(Al_{2.99}V_{0.01})Si_3O_{12}OH$
[e]$(Ca_{1.99}Sr_{0.01})(Al_{2.88}Fe_{0.12})Si_3O_{12}OH$
[f]$Ca_{1.99}(Al_{2.87}Fe_{0.11})Si_{3.00}O_{12}OH$

(1997) (Fig. 3a–c), while the *b*-axis compressions in both studies are similar (Fig. 3b). The zoisite samples including the Fe-free and Fe-bearing investigated by Alvaro et al. (2012) show much different axial compressibilities (Table 5). Their *a*-axes are much stiffer compared to this study (Fig. 3a), while *b*- and *c*-axes are slightly more compressible (Fig. 3b, c).

The pressure dependences of the axial compressibilities were also compared with that of Alvaro et al. (2012) in Fig. 6, which indicates that $\beta_a < \beta_b < \beta_c$ is true over the entire pressure range, although the differences between them are getting smaller with increasing pressure. β_b and β_c decrease with increasing pressure for zoisites from this study and Alvaro et al. (2012). β_b in this study is smaller below ~4 GPa; after that, it is larger. β_c of Alvaro et al. (2012) is larger within 0 to ~7 GPa, and the differences decrease with increasing pressure. The dramatic difference in the axial compressibility between this study and Alvaro et al. (2012) is β_a. β_a of Alvaro et al. (2012) is much smaller than that of this study, and the former increases with increasing pressure (elastic softening), which is opposite to this study (Fig. 6).

The elastic softening is unusual in hydrous silicates (e.g., Miletich et al. 2014). Several studies have been conducted on the compressional behaviors of epidote and clinozoisite using the high-pressure XRD method combined with DACs, and these studies employed Ne or the methanol:ethanol:water (16:3:1) mixture as the pressure-transmitting media (Fan et al. 2011, 2014; Gatta et al. 2011; Qin et al. 2016). These studies indicate that the axial compressibilities of epidote and clinozoisite decrease with increasing pressure, which is consistent with this study of zoisite. Considering that the Fe-bearing sample ($X_{Fe} = 0.12$) of Alvaro et al. (2012) has a similar Fe content to this study (0.11) and the other chemical differences (like Sr) are also minor, such a compositional difference may not contribute to the dramatic difference in β_a. Alvaro et al. (2012) used a methanol:ethanol (4:1) mixture as the pressure-transmitting medium, while Ne was used in this study. The different pressure-transmitting media might be responsible for the inconsistency in β_a.

Implications

Epidote-group minerals including epidote, zoisite, and clinozoisite commonly occur in subduction-related metamorphic rocks from blueschist to eclogite rock faces, and geochemical studies on natural rocks and petrological experiments suggest that these hydrous minerals are the main hosts of trace elements (like Sr) in metabasic compositions (Hermann 2002; Nagasaki and Enami 1998; Spandler et al. 2003). The stabilities of these minerals thus strongly control the cycles of water and trace elements in the deep mantle, which could be associated with the hydration-induced partial melting reactions of the mantle wedge above the subducted slab (Forneris and Holloway 2003). At temperatures higher than 600 °C, epidote minerals would breakdown at shallow mantle *P*–*T* conditions, although the incorporation of trace elements can stabilize them to higher temperatures (Forneris and Holloway 2003; Hermann 2002). For instance, within the $CaO–Al_2O_3–SiO_2–H_2O$ system, zoisite can stabilize to 6.6 GPa at 950 °C, and it metastably stabilize to higher pressures requires lower temperatures (Poli and Schmidt 1998; Schmidt and Poli 2004). Therefore, under most types of subduction zone *P*–*T* conditions, based on the previous experimental studies, epidote minerals cannot survive to depths greater than ~200 km

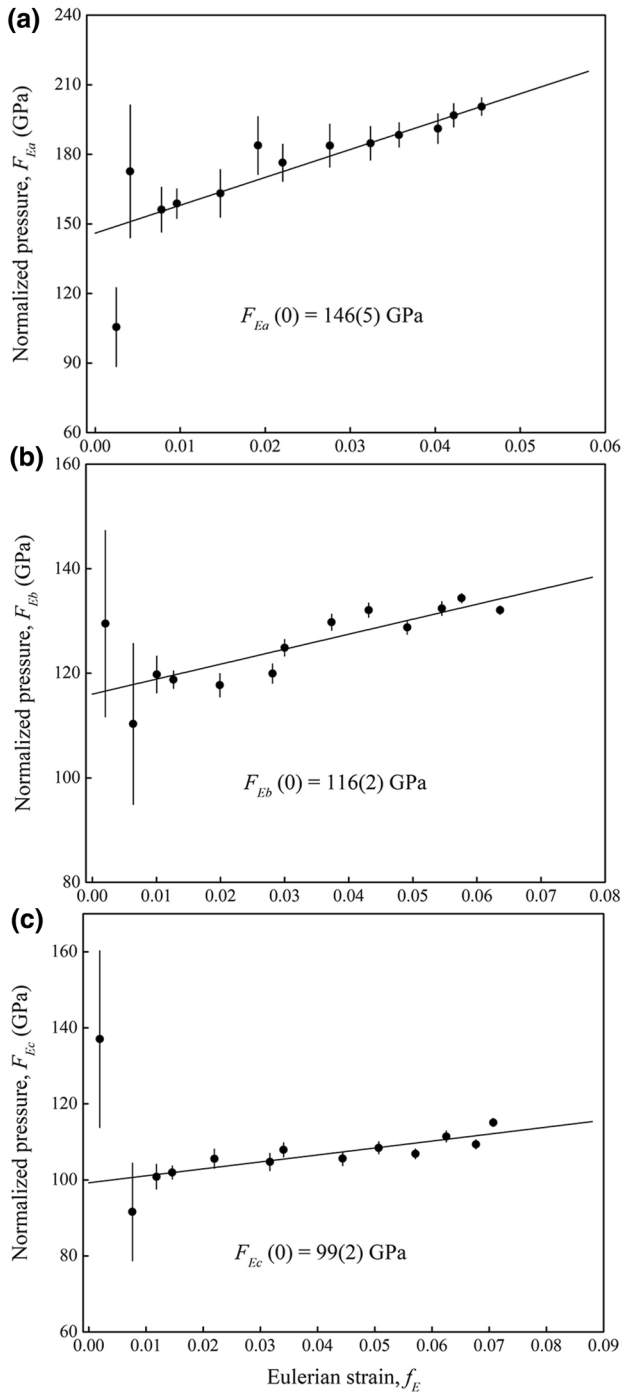

Fig. 5 Eulerian strain-normalized pressure (F_E–f_E) plot of the *a*- (**a**), *b*- (**b**), and *c*-axes (**c**) of zoisite. The straight lines represent the linear fits of the F_E–f_E data. The intercept values are F_E (0) = 146(5), 116(2), and 99(2) GPa for the *a*-, *b*-, and *c*-axes, respectively

Table 4 BM3 EoS-fitting coefficients and axial compressibilities of the zoisite lattice parameters *a, b*, and *c* in this study

	a	*b*	*c*
l_0 (Å)	16.2055(8)	5.5595(7)	10.0425(10)
K_{T0} (GPa)	147(6)	115(2)	98(2)
K'_{T0}	9.4(9)	5.8(3)	5.4(3)
β_0 (GPa^{-1})	0.00227(9)	0.00290(6)	0.00340(8)

(Forneris and Holloway 2003; Hacker et al. 2003; Poli and Schmidt 1998).

Alternatively, at ambient temperature, several high-pressure studies indicate that epidote-group minerals including epidote and clinozoisite are stable with no phase transitions up to at least 20 GPa (Fan et al. 2011, 2014; Gatta et al. 2011; Qin et al. 2016). In this study, the high-pressure single-crystal XRD experiments indicate that no phase transition occurs on the compression of zoisite to 34 GPa. Therefore, these studies may indicate that epidote-group minerals could metastably survive to larger depths under extremely cold subduction zone conditions (Ganguly et al. 2009). However, it should be noted that these studies do not prove that epidote minerals can be carriers for volatiles (like water) to the deep Earth, as they have not determined the presence of proton under DAC high-pressure conditions.

Conclusion

The compressional behavior of a natural eclogitic zoisite was investigated in a DAC combined with the synchrotron-based single-crystal XRD method. No phase transitions occur up to the maximum pressure of 34 GPa. The *P*–*V* data were fitted to a BM3 EoS and yielded $V_0 = 904.77(8)$ Å^3, $K_{T0} = 118(1)$ GPa, and $K'_{T0} = 6.3(2)$. The compression of zoisite is anisotropic, and the axial compressibilities at zero pressure (β_0) were determined to be 0.00227(9), 0.00290(6), and 0.00340(8) GPa^{-1} for *a*-, *b*- and *c*-axes, respectively, and over the experimental pressure range $\beta_{a0} < \beta_{b0} < \beta_{c0}$. Zoisite and other epidote minerals (like epidote and clinozoisite) cannot stabilize to depths greater than ~ 200 km under most subduction *P*–*T* conditions, while, at ambient-temperature conditions, these minerals can be stable to much higher pressures (at least 20 GPa). Therefore, under extremely cold subduction zones, epidote minerals might survive to greater depths.

Table 5 Axial compression anisotropy of zoisite

β_{a0}	β_{b0}	β_{c0}	β_{a0}:β_{b0}:β_{c0}	References
0.0023(2)	0.0029(1)	0.0037(2)	1:1.26:1.61	Comodi and Zanazzi (1997)
0.00137(3)	0.00314(6)	0.00375(2)	1:2.29:2.74	Alvaro et al. (2012), Fe-free
0.00134(2)	0.00314(3)	0.004006(2)	1:2.34:2.99	Alvaro et al. (2012), Fe-bearing
0.00227(9)	0.00290(6)	0.00340(8)	1:1.28:1.50	This study

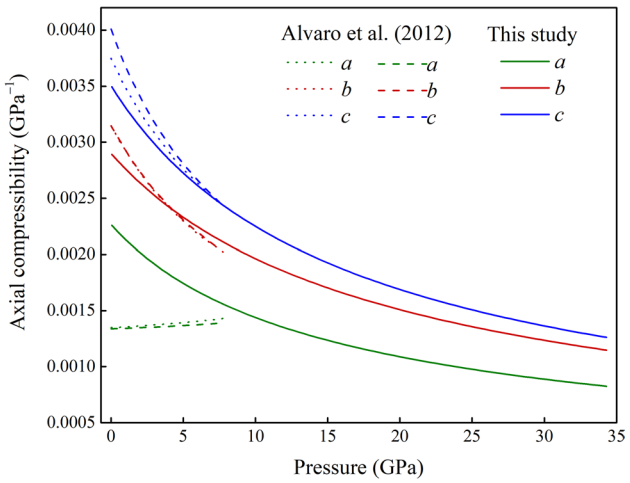

Fig. 6 Pressure dependences of axial compressibility of *a*-, *b*- and *c*-axes of zoisite. The dashed and dotted lines represent the Fe-free and Fe-bearing zoisite data (Alvaro et al. 2012), respectively. Weighted BM3 EoS fits are used to plot this figure (color online)

Acknowledgements We acknowledge Sergey N. Tkachev for the neon gas-loading assistance. This project was supported by the Chinese Academy of Sciences "Light of West China" Program (Dawei Fan, 2017), the National Natural Science Foundation of China (Grant No. 41802043 and 41772043), the Joint Research Fund in Huge Scientific Equipment (U1632112) under cooperative agreement between NSFC and CAS, Youth Innovation Promotion Association CAS (Dawei Fan, 2018434), and the CPSF-CAS Joint Foundation for Excellent Post-doctoral Fellows (Grant No. 2017LH014). The experimental work of this study was conducted at GeoSoilEnviroCARS (Sector 13), Partnership for Extreme Crystallography program (PX^2), Advanced Photon Source (APS), and Argonne National Laboratory. GeoSoilEnviroCARS is supported by the National Science Foundation—Earth Sciences (EAR-1128799) and Department of Energy—Geosciences (DE-FG02-94ER14466). PX^2 program is supported by COMPRES under NSF Cooperative Agreement EAR 11-57758. Use of the COMPRES-GSE-CARS gas-loading system was supported by COMPRES under NSF Cooperative Agreement EAR 11-57758 and by GSECARS. Development of the ATREX software used for data analysis is supported by NSF grant EAR1440005. Use of the Advanced Photon Source was supported by the US Department of Energy, Office of Science, Office of Basic Energy Sciences, under Contract No.DE-AC02-06CH11357. We would like to thank three anonymous reviewers for their thorough and helpful comments, which helped to improve the quality of this manuscript, and Prof. Larissa Dobrzhinetskaya for handling this manuscript.

References

Alvaro M, Angel RJ, Camara F (2012) High-pressure behavior of zoisite. Am Miner 97:1165–1176. https://doi.org/10.2138/am.2012.4014

Angel RJ (2000) Equations of state. Rev Miner Geochem 41:35–59

Angel RJ, Bujak M, Zhao J, Gatta GD, Jacobsen SD (2007) Effective hydrostatic limits of pressure media for high-pressure crystallographic studies. J Appl Crys 40:26–32

Angel RJ, Gonzalez-Platas J, Alvaro M (2014) EosFit7c and a Fortran module (library) for equation of state calculations. Z Kristallogr 229:405–419. https://doi.org/10.1515/zkri-2013-1711

Bina CR, Navrotsky A (2000) Possible presence of high-pressure ice in cold subducting slabs. Nature 408:844–847. https://doi.org/10.1038/35048555

Boettcher A (1970) The system CaO-Al_2O_3-SiO_2-H_2O at high pressures and temperatures. J Petrol 11:337–379

Comodi P, Zanazzi PF (1997) The pressure behavior of clinozoisite and zoisite: An X-ray diffraction study. Am Mineral 82:61–68

Dera P, Zhuravlev K, Prakapenka V, Rivers ML, Finkelstein GJ, Grubor-Urosevic O, Tschauner O, Clark SM, Downs RT (2013) High pressure single-crystal micro X-ray diffraction analysis with GSE_ADA/RSV software. High Press Res 33:466–484

Dollase WA (1968) Refinement and comparison of the structures of zoisite and clinozoisite. Am Miner 53:1882–1898

Dolomanov OV, Bourhis LJ, Gildea RJ, Howard JA, Puschmann H (2009) OLEX2: a complete structure solution, refinement and analysis program. J Appl Crystallogr 42:339–341

Dörsam G, Liebscher A, Wunder B, Franz G, Gottschalk M (2007) Crystal chemistry of synthetic $Ca_2Al_3Si_3O_{12}OH$–$Sr_2Al_3Si_3O_{12}OH$ solid-solution series of zoisite and clinozoisite. Am Miner 92:1133–1147

Enami M, Liou J, Mattinson C (2004) Epidote minerals in high P/T metamorphic terranes: subduction zone and high-to ultrahigh-pressure metamorphism. Rev Miner Geochem 56:347–398

Fan D, Ma M, Yang J, Wei S, Chen Z, Xie H (2011) In situ high-pressure synchrotron X-ray diffraction study of clinozoisite. Chin Phys Lett 28. https://doi.org/10.1088/0256-307x/28/12/126103

Fan D, Xu J, Wei S, Chen Z, Xie H (2014) In situ high-pressure synchrotron X-ray diffraction of natural epidote. Chin J High Press Phys 28:257–261

Fei YW, Ricolleau A, Frank M, Mibe K, Shen G, Prakapenka V (2007) Toward an internally consistent pressure scale. Proc Natl Acad Sci USA 104:9182–9186

Fesenko E, Rumanova I, Belov N (1955) The crystal structure of zoisite. Structure Reports 19:464–465

Forneris JF, Holloway JR (2003) Phase equilibria in subducting basaltic crust: implications for H_2O release from the slab. Earth Planet Sci Lett 214:187–201

Franz G, Liebscher A (2004) Physical and chemical properties of the epidote minerals—an introduction. Rev Miner Geochem 56:1–81

Ganguly J, Freed AM, Saxena SK (2009) Density profiles of oceanic slabs and surrounding mantle: Integrated thermodynamic and thermal modeling, and implications for the fate of slabs at the 660 km discontinuity. Phys Earth Planet Inter 172:257–267

Gatta GD, Merlini M, Lee Y, Poli S (2011) Behavior of epidote at high pressure and high temperature: a powder diffraction study up to 10 GPa and 1,200 K. Phys Chem Miner 38:419–428

Ghose S, Tsang T (1971) Ordering of V^{2+}, Mn^{2+}, and Fe^{3+} ions in zoisite, $Ca_2Al_3Si_3O_{12}(OH)$. Science 171:374–376

Gonzalez-Platas J, Alvaro M, Nestola F, Angel R (2016) EosFit7-GUI: a new graphical user interface for equation of state calculations, analyses and teaching. J Appl Crystallogr 49:1377–1382

Grevel KD, Nowlan EU, Fasshauer DW, Burchard M (2000) In situ X-ray diffraction investigation of lawsonite and zoisite at high pressures and temperatures. Am Miner 85:206–216

Hacker BR, Peacock SM, Abers GA, Holloway SD (2003) Subduction factory 2. Are intermediate-depth earthquakes in subducting slabs linked to metamorphic dehydration reactions? J Geophys Res 108:2030

Hermann J (2002) Allanite: thorium and light rare earth element carrier in subducted crust. Chem Geol 192:289–306

Klotz S, Chervin J, Munsch P, Le Marchand G (2009) Hydrostatic limits of 11 pressure transmitting media. J Phys D 42:075413

Liebscher A, Gottschalk M, Franz G (2002) The substitution Fe^{3+}-Al and the isosymmetric displacive phase transition in synthetic zoisite: a powder X-ray and infrared spectroscopy study. Am Miner 87:909–921

Mao Z, Jiang F, Duffy TS (2007) Single-crystal elasticity of zoisite $Ca_2Al_3Si_3O_{12}(OH)$ by Brillouin scattering. Am Miner 92:570–576

Miletich R et al (2014) Cordierite under hydrostatic compression: Anomalous elastic behavior as a precursor for a pressure-induced phase transition. Am Miner 99:479–493

Momma K, Izumi F (2011) VESTA 3 for three-dimensional visualization of crystal, volumetric and morphology data. J Appl Crystallogr 44:1272–1276

Nagasaki A, Enami M (1998) Sr-bearing zoisite and epidote in ultrahigh pressure (UHP) metamorphic rocks from the Su-Lu province, eastern China; an important Sr reservoir under UHP conditions. Am Miner 83:240–247

Nesse WD (2000) Introduction to mineralogy. Oxford University Press, New York

Nicholls I, Ringwood A (1973) Effect of water on olivine stability in tholeiites and the production of silica-saturated magmas in the island-arc environment. J Geol 81:285–300

Pawley A, Chinnery N, Clark S (1998) Volume measurements of zoisite at simultaneously elevated pressure and temperature. Am Miner 83:1030–1036

Poli S, Schmidt M (1998) The high-pressure stability of zoisite and phase relationships of zoisite-bearing assemblages. Contri Miner Petrol 130:162–175

Qin F, Wu X, Wang Y, Fan D, Qin S, Yang K, Townsend JP, Jacobsen SD (2016) High-pressure behavior of natural single-crystal epidote and clinozoisite up to 40 GPa. Phys Chem Miner 43:649–659

Rivers M, Prakapenka VB, Kubo A, Pullins C, Holl CM, Jacobsen SD (2008) The COMPRES/GSECARS gas-loading system for diamond anvil cells at the Advanced Photon Source. High Press Res 28:273–292

Schmidt MW, Poli S (2004) Magmatic epidote. Rev Miner Geochem 56:399–430

Sheldrick GM (2008) A short history of SHELX. Act Crystallogr 64:112–122

Spandler C, Hermann J, Arculus R, Mavrogenes J (2003) Redistribution of trace elements during prograde metamorphism from lawsonite blueschist to eclogite facies; implications for deep subduction-zone processes. Contri Miner Petrol 146:205–222

Zhang D, Dera PK, Eng PJ, Stubbs JE, Zhang JS, Prakapenka VB, Rivers ML (2017) High pressure single crystal diffraction at PX^2. J Visual Exper JoVE. https://doi.org/10.3791/54660